C. R. Physique 3 (2002) 365–380

Solides, fluides : propriétés magnétiques et électriques/*Solids, fluids: magnetic and electrical properties*
(Solides, fluides : structure/*Solids, fluids: structure*)

DOSSIER

AGRÉGATS COMME PRÉCURSEURS DES NANO-OBJETS
CLUSTERS AS PRECURSORS OF NANO-OBJECTS

Ultrafast electron interactions in metal clusters

Natalia Del Fatti, Fabrice Vallée

CPMOH, CNRS-Université Bordeaux I, 351, cours de la libération, 33405 Talence, France

Received 28 January 2002; accepted 3 February 2002

Note presented by Guy Laval.

Abstract The recent extension of time-resolved femtosecond optical techniques to the investigation of the ultrafast electron scattering processes in metal clusters offers the unique possibility to follow their evolution from a bulk to a confined metal. The size dependent results obtained in model materials, the noble metals, are presented, focusing on the impact of the confinement on energy redistribution processes (electron–electron and electron–phonon coupling). Their application to the investigation of the acoustic vibration property of cluster and to the cluster-surrounding matrix energy transfers are also discussed. ***To cite this article: N. Del Fatti, F. Vallée, C. R. Physique 3 (2002) 365–380.*** © 2002 Académie des sciences/Éditions scientifiques et médicales Elsevier SAS

metal cluster / femtosecond spectroscopy / electron interaction

Interactions électroniques ultrarapides dans des agrégats métalliques

Résumé L'extension récente des techniques femtosecondes résolues en temps à l'étude des mécanismes d'interaction électronique dans les agrégats métalliques permet de suivre leur évolution d'un métal massif à un métal confiné. Les resultats obtenus en fonction de la taille dans des matériaux modèles, les métaux nobles, sont présentés, en nous focalisant sur l'impact du confinement sur les processus de redistribution de l'énergie (couplages électrons–électrons et électrons–phonons). Leurs applications à l'étude des propriétés des vibrations acoustiques des agrégats et du transfert d'énergie agrégat-matrice sont également discutées. ***Pour citer cet article : N. Del Fatti, F. Vallée, C. R. Physique 3 (2002) 365–380.*** © 2002 Académie des sciences/Éditions scientifiques et médicales Elsevier SAS

agrégats métalliques / spectroscopie femtoseconde / interactions électronique

1. Introduction

Understanding and modeling the new physical properties exhibited by nanomaterials has been an intense field of research during the last decades. This is motivated by both the fundamental interest, nanoparticles or clusters constituting intermediate systems between molecules and bulk materials, and the technological relevance, nanostructured systems being a very important class of new materials for technological applications. The interaction processes inside a cluster (scattering of electrons between

E-mail addresses: delfatti@cribx1.u-bordeaux.fr (N. Del Fatti); fvallee@cribx1.u-bordeaux.fr (F. Vallée).

S1631-0705(02)01317-8/FLA

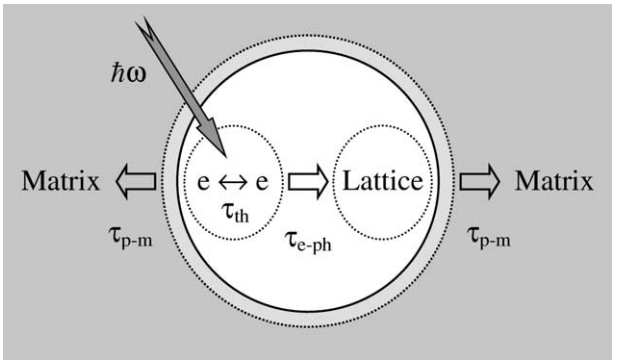

Figure 1. Sketch of the energy relaxation processes after selective excitation of nonequilibrium electrons by a femtosecond pulse ($\hbar\omega$) in a metal cluster embedded in a matrix. τ_{th} and $\tau_{\mathrm{e-ph}}$ are the characteristic times for electron–electron and electron–lattice energy exchanges in a nanoparticle, respectively. $\tau_{\mathrm{p-m}}$ is the nanoparticle–environment energy exchange time.

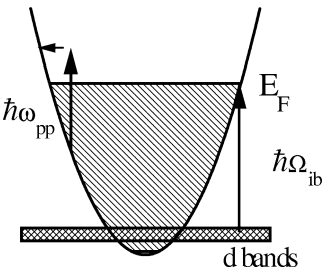

Figure 2. Schematic band structure of noble metals with intraband excitation at $\hbar\omega_{\mathrm{pp}}$. $\hbar\Omega_{\mathrm{ib}}$ is the threshold for the interband transitions from the d-bands to empty states above the Fermi energy E_{F}.

themselves and with the lattice) and its coupling with the environment (surrounding matrix, adsorbed molecules, other nanoparticles,...) play here a key role. However, they are difficult to address with conventional experimental techniques. With the advance of femtosecond lasers, they can now be selectively investigated using time-resolved optical techniques that have emerged as powerful tools for the analysis and understanding of the fundamental interaction mechanisms of the elementary excitations in dense matter.

In the case of metallic materials, these techniques are based on selective electron excitation by an optical pump pulse, on a time scale shorter than that of the electron–electron and/or electron–lattice energy redistributions reviewed in [1]. The injected energy is subsequently redistributed among the electrons by electron–electron (e–e) scattering in few hundred femtoseconds [1–8], transferred to the lattice by electron–phonon (e–ph) interaction in typically one picosecond [2–4,9,10], and eventually damped to the environment in few to few hundred picoseconds (Fig. 1) [11–13]. These different steps of nonequilibrium electron relaxation are followed by a time-delayed probe pulse monitoring the time-evolution of an optical property of the material that depends on the electron energy distribution or lattice temperature, i.e., modified by electron excitation by the pump pulse. This approach, that exploits the material ultrafast electronic optical nonlinearities, was first used in bulk metal [1]. It has been recently extended to nanomaterials formed by nanoparticles dispersed in a matrix or deposited on a substrate [14–20]. New problems have thus been addressed in clusters: ultrafast electron interactions (e–e and e–ph energy exchanges), acoustic vibrations, and energy exchanges with the matrix [14]. It opens a new area in the physics of clusters: investigation of the interaction mechanisms of their elementary excitations and with their environment.

In this paper we discuss the results obtained in large spherical nanoparticles of noble metals (diameter $D \geqslant 2$ nm, i.e., more than few hundred atoms). Their relatively simple band structure (Fig. 2) and the simple connection between their optical properties and their electron energy distribution, make them model systems for these studies. We will focus on the low perturbation regime investigations since in these conditions, the nanoparticle nonlinear optical response can be modeled simply and the results obtained for different sizes compared directly. Furthermore, as these not too small metal objects can be conveniently described using a small solid approach, rather than a molecular one for few atom clusters, their responses

can also be directly compared to those of the bulk material. This permits us to trace the first impacts of confinement on the electron interaction processes and ultrafast nonlinear optical response of metals [21].

2. Optical properties of metal clusters

The optical properties of a composite material formed by small metal clusters ($D \ll \lambda$, where λ is the optical wavelength), dispersed in a solid or liquid matrix or deposited on a substrate can be described by introducing an effective dielectric constant [11,22–25]

$$\widetilde{\varepsilon}(\omega) = \varepsilon_d + 3p\,\varepsilon_d\,\frac{\varepsilon(\omega) - \varepsilon_d}{\varepsilon(\omega) + 2\varepsilon_d} \tag{1}$$

where $p \ll 1$ is the metal volume fraction. $\varepsilon(\omega) = \varepsilon_1(\omega) + \mathrm{i}\varepsilon_2(\omega)$ and ε_d are the dielectric constants of the metal nanoparticles and matrix, respectively. The latter is assumed frequency independent and real in the spectral range of interest. The absorption coefficient can then be written [24,25]:

$$\widetilde{\alpha}(\omega) = \frac{9\,p\,\varepsilon_d^{3/2}}{c}\,\frac{\omega\,\varepsilon_2(\omega)}{[\varepsilon_1(\omega) + 2\varepsilon_d]^2 + \varepsilon_2^2(\omega)} \tag{2}$$

As compared to the bulk metal, the absorption is resonantly enhanced close to the frequency, Ω_R, minimizing the denominator. This is the well known condition for the surface plasmon resonance (SPR). This is concomitant with enhancement of the electric field inside the particle as compared to the applied field and can be described in terms of a local field effect [11,24]. The same effect is responsible for the enhancement of the nonlinear optical response which, as in bulk metal, is still directly connected to the electron distribution dependence of $\varepsilon(\omega)$.

The dielectric constant of bulk metals can be separated into conduction and bound electron contributions. In noble metals, the former is well described by a Drude formula (free electron response) [26] and ε can be written:

$$\varepsilon(\omega) = \varepsilon^b(\omega) - \frac{\omega_p^2}{\omega[\omega + \mathrm{i}/\tau(\omega)]} \tag{3}$$

where $\tau(\omega)$ is the electron optical relaxation time and ω_p the plasma frequency ($\omega_p^2 = n_e e^2/\varepsilon_0 m$, where n_e is the conduction electron density). ε^b is the bound electron contribution, related to interband absorption, i.e., transitions from the full d-bands to empty states in the conduction band in noble metals (Fig. 2) [27].

In a nanocrystal, the response of the conduction electrons is modified by their quantum confinement, or, classically, using a small solid model, by electron scattering off the surface. Using either approach, one can show that their contribution to ε preserves its Drude form with a modified size-dependent scattering time $\tau(\omega, D)$ [11,20,22,24,28]. For not too small particles ($D \geqslant 3$ nm), modification of the interband transition spectrum can be neglected [29]. The nanocrystallite dielectric constant can thus be obtained by using the measured bulk metal dielectric constant [26] and introducing the surface correction as a parameter to reproduce the measured absorption spectra (Fig. 3) [14]. This expression for ε will be used in the following.

Because of the large frequency threshold for the interband transitions in silver ($\hbar\Omega_{\mathrm{ib}} \approx 4$ eV), the SPR lies in an isolated region of the spectrum and shows up as a well defined resonance (Fig. 3). This is in contrast to other metals where the SPR overlaps the interband transitions, making Ag a model material for investigating the influence of confinement on the ultrafast nonlinear optical response and electron kinetics.

3. Optical creation of nonequilibrium electrons

The first step in ultrafast optical investigations of metals is to create a nonequilibrium electron distribution. It can be done either by intraband (free electron) or interband absorption of a femtosecond

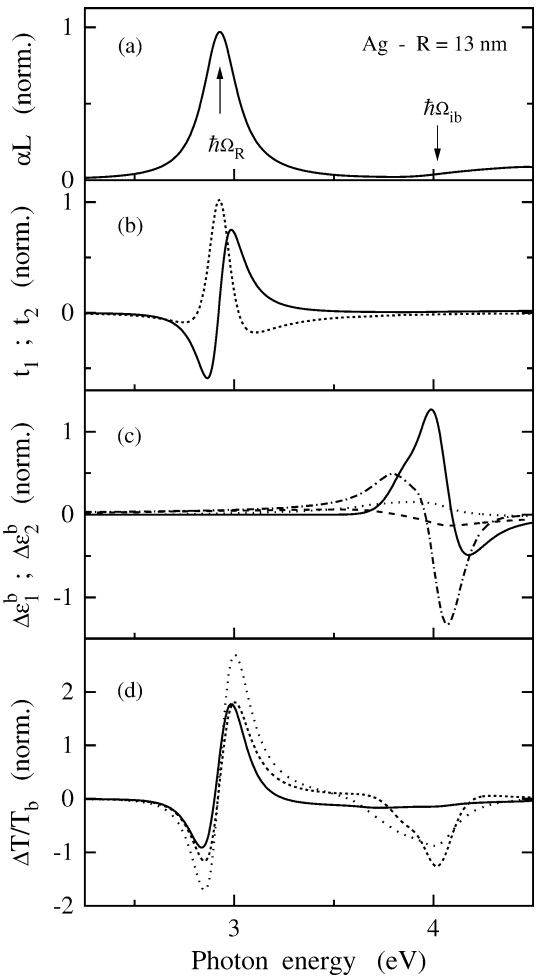

Figure 3. (a) Fit to the measured absorption spectra of $R = 13$ nm silver nanoparticles in glass. The SPR frequency ($\hbar\Omega_R = 2.93$ eV) and interband transition threshold ($\hbar\Omega_{ib} \approx 4$ eV) are indicated. (b) Dispersion of the coefficients t_1 (full line) and t_2 (dashed line) linking $\Delta T/T$ to $\Delta\varepsilon_1$ and $\Delta\varepsilon_2$ (6) for the same sample. (c) Interband contribution to $\Delta\varepsilon_1$ and $\Delta\varepsilon_2$ calculated for $t_D = 0$ fs (dashed and dotted lines) and $t_D = 500$ fs (dash–dotted and full lines) for excitation with a 25 fs near infrared pulse and $\Delta T_e^{me} = 100$ K. (d) Corresponding transmission change due to the interband contribution for $t_D = 0$, 100 and 500 fs (full, dotted and dashed line, respectively).

pump pulse. If its frequency ω_{pp} is smaller than the interband transition threshold Ω_{ib}, only the former process is effective. Excitation thus takes place at constant electron density in the bands. Coherent coupling of the pump-pulse electromagnetic field and electron motion takes place initially, the induced polarization decaying with electron scattering in agreement with time-resolved nonlinear investigations [30–32] and hole burning measurements [32]. This process is described by the imaginary part of the Drude term of the dielectric function and is determined by electron scattering with simultaneous exchange of a photon of energy $\hbar\omega_{pp}$.

It leads to the creation of electron-hole pairs in the conduction band on a sub-20 fs scale [33], where electrons with an energy E between $E_F - \hbar\omega_{pp}$ and E_F are excited above the Fermi energy with a final energy between E_F and $E_F + \hbar\omega_{pp}$ (Fig. 4). For an isotropic conduction band, the pump-induced change of the conduction electron occupation number f can be written [2]:

$$\Delta f_{exc}(E,t) = AI_p(t)\big\{\sqrt{E-\hbar\omega_{pp}}\, f(E-\hbar\omega_{pp})\big[1-f(E)\big] - \sqrt{E+\hbar\omega_{pp}}\, f(E)\big[1-f(E+\hbar\omega_{pp})\big]\big\} \quad (4)$$

where $I_p(t)$ is the pump pulse intensity and A a constant proportional to the injected energy. It is usually characterized by defining an equivalent electron temperature rise ΔT_e^{me}, i.e., the temperature increase of a thermalized electron gas for the same injected energy.

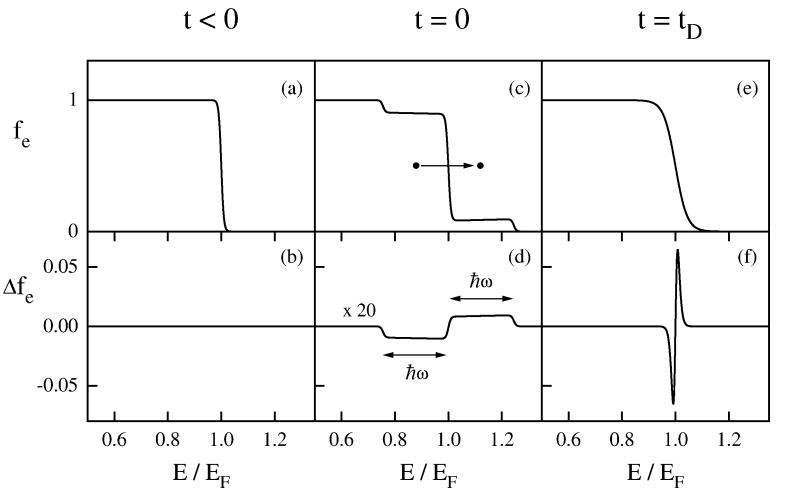

Figure 4. Energy dependent electron occupation number before excitation, $t < 0$ (equilibrium f_0) (a), during excitation $t = 0$ assuming instantaneous intraband excitation by a pump pulse of frequency ω_{pp}, with $\hbar\omega_{pp} = 0.24E_F$ (athermal f) (c) and after establishment of an electron temperature after a delay $t = t_D > 0$ (e). (b), (d) and (f) are the corresponding distribution changes $\Delta f = f - f_0$ for $\Delta T_e^{me} = 100$ K (the same total electron energy is assumed for (d) and (f)).

When interband absorption takes place, i.e., for $\hbar\omega_{pp} \geqslant \hbar\Omega_{ib}$, the number of electrons in the conduction band increases. However, the created d-band holes recombine in a few tens of femtoseconds via an Auger process leading to indirect conduction electron excitation [6,34]. This first step has to be taken into account when electron scattering on the few first tens of femtoseconds is studied, the subsequent longer time scale electron dynamics being very similar for intra and interband absorptions. For the sake of simplicity, only intraband excitation will be considered here.

Neglecting exchanges with the environment, that usually take place on a longer time scale, electron–electron (e–e) and electron–phonon (e–ph) interactions redistribute the injected energy in each nanoparticle, eventually leading to a thermalized electron–lattice system. The lattice heat capacity being much larger than the electronic one, a large transient electron perturbation can be achieved with only a small lattice heating when the system eventually reaches quasi-equilibrium. In bulk metals, the time evolution of the conduction electron energy distribution function f can be described by the Boltzmann equation [2,4,35,36]:

$$\frac{\mathrm{d}f(E)}{\mathrm{d}t} = \left.\frac{\mathrm{d}f(E)}{\mathrm{d}t}\right|_{\mathrm{e-e}} + \left.\frac{\mathrm{d}f(E)}{\mathrm{d}t}\right|_{\mathrm{e-ph}} + \Delta f_{\mathrm{exc}}(E,t) \tag{5}$$

The electron distribution changes computed in bulk silver for a pump photon energy $\hbar\omega_{pp} = 1.3$ eV and a 25 fs pulse duration are shown in Fig. 3, for $\Delta T_e^{me} = 100$ K (corresponding to our experimental conditions). Δf initially extends over a very broad energy range ($t_D = 0$ in Fig. 3) and subsequently strongly narrows as the electron gas internally thermalizes ($t_D = 1$ ps in Fig. 3). It has been shown that this kinetics is independent of the injected energy in the weak perturbation regime, i.e., for $\Delta T_e^{me} \leqslant 200{-}300$ K, greatly simplifying the interpretation of the experimental results [4]. For larger energy injection, it strongly depends on the excitation amplitude making extraction of the intrinsic electron interaction parameters difficult.

4. Optical probing of the electron kinetics

The changes of the material optical properties induced by modification of the electron distribution can be followed using a second time-delayed femtosecond probe pulse at the frequency ω_{pr} that monitors the sample transmission $\Delta T(\omega_{pr}, t_D) = T(\omega_{pr}, t_D) - T(\omega_{pr}, -\infty)$ or reflection $\Delta R(\omega_{pr}, t_D) = R(\omega_{pr}, t_D) - R(\omega_{pr}, -\infty)$ where t_D is the pump-probe delay. For a sufficiently weak excitation, a perturbative approach

can be used [2]. In a dilute composite material the normalized transmission change $\Delta T/T$ is only determined by $\Delta\widetilde{\varepsilon}_2(\omega_{\rm pr}, t_D)$, or, equivalently, by the sample absorption change [14]:

$$\Delta T/T(\omega_{\rm pr}, t_D) = -\Delta\widetilde{\alpha}(\omega_{\rm pr}, t_D)L = t_1\Delta\varepsilon_1(\omega_{\rm pr}, t_D) + t_2\Delta\varepsilon_2(\omega_{\rm pr}, t_D) \tag{6}$$

where L is the sample thickness. The $\omega_{\rm pr}$ dependent t_1 and t_2 coefficients are entirely determined by the unperturbed material dielectric function and the ε dependence of $\widetilde{\alpha}$ (2). Information on the electron kinetics can thus be obtained from the time dependence of ΔT, provided that $\Delta\varepsilon$ is connected to the transient electron distribution change Δf.

In noble metals, the interband contribution to $\Delta\varepsilon$ dominates the short time scale response (3). Around the interband transition threshold $\hbar\Omega_{\rm ib}$, the interband absorption spectrum is determined by the occupation of the electronic states close to $E_{\rm F}$ and is thus modified by electron distribution smearing induced by the pump pulse (Fig. 4) [2,4]. To quantitatively describe this effect for interpreting CW thermomodulation measurements, Rosei and co-workers modeled the bulk noble metal band structure around the Brillouin zone points contributing to the absorption [37]. This model permits the linking of $\Delta\varepsilon_2^b$ to Δf, $\Delta\varepsilon_1^b$ being then obtained by Kramers–Kronig transformation. We have used this approach to model the femtosecond response of noble metals using a time dependent Δf obtained by numerically solving the Boltzmann equation (5) [2–4,14,20]. The $\Delta\varepsilon_1^b$ and $\Delta\varepsilon_2^b$ spectra computed for $t_D = 0$ and 500 fs are shown in Fig. 3 for bulk silver [4,14].

For not too small particles the same approach can be used to compute $\Delta\varepsilon^b$. As a first approximation, assuming that its time evolution is unchanged in nanoparticles (which turns out to be wrong for the smallest ones) the interband contribution $(\Delta T/T)_b$ to $\Delta T/T$ is obtained using (6) (Fig. 3), the difference with the bulk response lying in the coefficient t_1 and t_2 linking $\Delta T/T$ to $\Delta\varepsilon$ (6). In silver, the computed $(\Delta T/T)_b$ exhibits two distinct spectral features around $\Omega_{\rm ib}$ and Ω_R with very different time behaviors (Fig. 3). The former is similar to that observed in the bulk material and corresponds to resonant probing of the interband transitions. Its time behavior is related to the internal electron thermalization dynamics (Section 5). In contrast, the structure around Ω_R is a consequence of the well known confinement induced enhancement of the nonlinear optical response around the SPR [11], which, in our approach, reflects in the large amplitude and dispersion of t_1 and t_2 around Ω_R. In this spectral region, $\Delta\varepsilon^b$, i.e., the bulk metal response, is small and almost undispersed since it corresponds to probing away from the interband transitions. Its dynamics essentially reflects that of the electron gas energy, yielding information on electron–lattice coupling (Section 6). This clear frequency separation of the interband and confinement induced resonances in the nonlinear optical response only takes place in silver. In other metals, these features overlap making their time-dependent optical response more complex [14].

5. Electron–electron scattering

Electron–electron scattering and the correlated internal thermalization dynamics of the conduction electrons has been investigated in bulk gold and silver taking advantage of the sensitivity of the interband absorption around $\Omega_{\rm ib}$ on the electron occupation number change around $E_{\rm F}$ [2,4]. Electron internal thermalization is concomitant with a build-up of Δf close to $E_{\rm F}$ (Fig. 3) and thus of $(\Delta T/T)_b$ around $\Omega_{\rm ib}$. In this frequency range, $\Delta T/T$ is thus very sensitive to the thermal or athermal character of the distribution [2,4] and thus to its evolution to a Fermi–Dirac distribution (i.e., establishment of the electron temperature, T_e).

The situation is similar in large silver clusters, their absorption around $\Omega_{\rm ib}$ being almost unaffected by confinement (for $D \geqslant 3$ nm). This is backed-up by the very good agreement between the spectral shape of the measured $-\Delta T/T$ and computed $(\Delta T/T)_b$ (Fig. 5).Using the same approach it is thus possible to follow the internal electron thermalization dynamics and to compare it for different particle sizes, i.e., to analyze the impact of confinement on the electron–electron interactions [38].

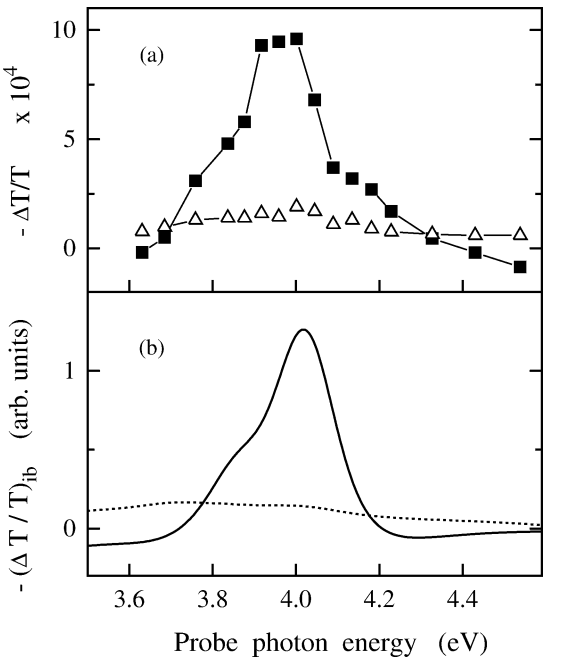

Figure 5. (a) Change of transmission $-\Delta T/T$ measured around the interband transition threshold for pump-probe delays of 0 fs (triangles) and 400 fs (squares) in $D = 6$ nm Ag nanoparticle. (b) Interband contribution $-(\Delta T/T)_b$ to $-\Delta T/T$ computed in the same conditions (dashed and full lines, respectively).

As in films, a delayed rise of $\Delta T/T$ has been observed, demonstrating a slow internal thermalization on a few hundred femtosecond scale. A characteristic internal thermalization time τ_{th} has been defined by fitting the measured signal around its maximum amplitude ($\hbar\omega_{\text{pr}} \approx 4$ eV), assuming a response function of the form [2,4,38]:

$$u(t) = H(t)\left[1 - \exp\left(-\frac{t}{\tau_{\text{th}}}\right)\right]\exp\left(-\frac{t}{\tau^0_{\text{e-ph}}}\right) \tag{7}$$

where $H(t)$ is the Heaviside function (Fig. 6). The exponential decay with the time $\tau^0_{\text{e-ph}}$ stands for electron energy transfer to the lattice [20]. For $D \geqslant 10$ nm, τ_{th} is close to its film value ($\tau_{\text{th}} \approx 350$ fs [4]) and strongly decreases for smaller sizes. This effect is independent of the cluster environment and excitation conditions (Fig. 7) [14,38], demonstrating an intrinsic confinement induced fastening of the electron–electron energy exchanges [38].

Similar measurements were performed in gold colloids with $D = 9$ to 48 nm, by El-Sayed et al. [15]. A delayed signal rise has also been observed around Ω_{ib} yielding τ_{th} values almost identical to that of the the bulk material ($\tau_{\text{th}} \approx 500$ fs [2]). This absence of variation in this size range is consistent with our silver results and has been confirmed by our recent investigations showing that τ_{th} exhibits a similar size dependence in gold and in silver clusters.

It has been shown in bulk metal that τ_{th} is essentially determined by e–e collisions around the Fermi surface. Their probabilities are strongly reduced by the Pauli exclusion principle effects making them the slowest scattering processes involved in the internal thermalization [2,4]. The experimental results have been found to be in quantitative agreement with the computed ones describing e–e scattering by a statically screened Coulomb potential, with phenomenologic screening reduction [2,4]. For a weak perturbation, the dependence of τ_{th} on n_e and core electron screening amplitude (related to $\varepsilon_{\text{sc}} = \varepsilon_1^b(0)$) is yielded by that of the scattering time of an electron out of its state τ_e [4,39]:

$$\tau_e \propto n_e^{5/6}\varepsilon_{\text{sc}}^{1/2} \tag{8}$$

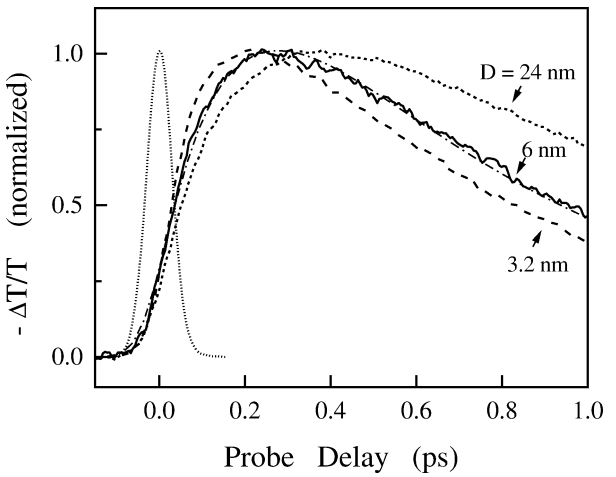

Figure 6. Time behavior of the transmission change $-\Delta T/T$ measured for $\hbar\omega_{\mathrm{pr}} \approx 3.95$ eV and $\hbar\omega_{\mathrm{pp}} \approx 1.32$ eV in spherical Ag nanoparticles of diameter $D = 24$ nm and 6 nm in $BaO–P_2O_5$ and $D = 3.2$ nm in Al_2O_3. The dash–dotted line is a fit for the $D = 6$ nm case using (7) and the dotted line the pump-probe cross-correlation.

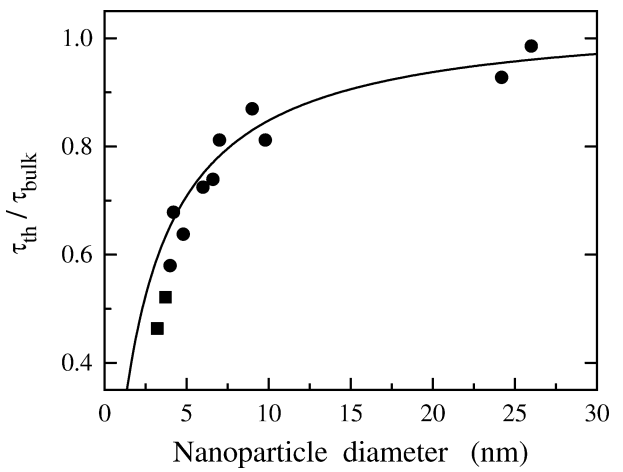

Figure 7. Size dependence of the electron thermalization time τ_{th} for Ag nanoparticles in a $BaO–P_2O_5$ (dots) and Al_2O_3 (squares) matrix. The full line shows the computed τ_{th} taking into account both the spillout and d-electron localization effects (from [38]).

This dependence quantitatively explains the faster electron scattering measured in bulk silver than in gold (350 fs as compared to 500 fs), d-band electron screening being large in the latter [4].

The τ_{th} size dependence has been ascribed to the intrinsic confinement induced fastening of the electron–electron energy exchanges, due to less efficient screening of the e–e Coulomb interactions close to a surface [38]. It has been shown that the wave functions of the conduction electrons extend beyond the particle radius defined by the ionic lattice (electron spillout [40]). This leads to an effective reduction of their density n_e and thus of ω_p. It manifests itself by a red shift of the SPR with size reduction in alkali metal clusters [41]. Conversely, the d-electron wave-functions are localized in the inner region of the particle leading to an incomplete embedding of the conduction electrons in the core electron background [42,43]. Both effects reduce the efficiency of the screening of the e–e Coulomb interactions. Using this model and the modeled spatial variations of $\varepsilon_{\mathrm{sc}}$ and n_e in a cluster, a good reproduction of the experimental τ_{th} size dependence was obtained (Fig. 7). It actually essentially reflects enhancement of the e–e scattering close to the metal surface.

The above model, based on a simple extension of the bulk calculations, overlooks specific features of the confined materials. In particular, the e–e scattering rate has been derived using the bulk electron wave functions and includes momentum conservation. This is relaxed in confined systems, due to, classically, electron scattering off the surfaces leading to opening of additional e–e scattering channels, i.e., further size

dependent modifications of the e–e interactions (this effect is comparable to the increase of the electron optical scattering rate due to surface effects). A more correct description requires nonlocal calculations of the e–e scattering rate and many body effects in a nanoparticle using the confined electron wave functions.

These first measurements open-up many possibilities for the investigation of quantum confinement effect on electron kinetics and interactions. In particular, their extension to other metals or type of confinement (1D or 2D systems) and the use of other techniques, such as time-resolved photoemission [44], would be particularly interesting.

6. Electron–lattice interaction

The transient signals measured in metallic systems decay in a few picoseconds with the electron gas excess energy and thus contain information on the energy exchanges of the electrons with their environment. In the case of films, this is essentially limited to the metal lattice, permitting direct measurement of the electron–phonon interaction time (i.e., the energy transfer time as defined using the two-temperature model, Eq. (9)). For nanoparticles the electron energy can also be damped to the surrounding solvent or matrix either directly or via the metal lattice, possibly modifying the observed relaxation. This coupling is frequently assumed to be sufficiently slow to be neglected on the scale of the metal electron–lattice energy exchange. However, it strongly increases with size reduction and may play a role in the observed electron cooling, especially for large electron excitation [45,46].

As long as only energy exchanges inside a nanoparticle are considered, they can be described using the bulk metal two-temperature model [47]. This is based on the assumption that both the electron and lattice are thermalized at different temperatures T_e and T_L and can only be used after internal electron thermalization, i.e., few hundred femtoseconds to one picosecond. The electron gas is then entirely described by its temperature and its cooling dynamics can be simply modeled using the rate equation system:

$$\begin{aligned} C_e(T_e)\left(\frac{\partial T_e}{\partial t}\right) &= -G(T_e - T_L) \\ C_L\left(\frac{\partial T_L}{\partial t}\right) &= G(T_e - T_L) \end{aligned} \tag{9}$$

where G is the effective electron–phonon coupling constant. For a weak perturbation, $\Delta T_e^{me} \ll T_0$ where T_0 is the initial temperature, $C_e(T_e)$ can be identified with $C_e(T_0)$ leading to an exponential decay of the electron temperature rise ΔT_e and of the electron excess energy Δu_e with the same time constant $\tau^0_{\mathrm{e-ph}} \approx C_e(T_0)/G$ [4]. The energy losses taking place on only a slightly longer time scale than internal thermalization, both effects can influence the measured temporal shapes. In noble metals, when probing away from the interband transition, the amplitude of the optical property change is almost independent of the exact electron distribution and proportional to Δu_e, permitting a precise determination of $\tau^0_{\mathrm{e-ph}}$ [3,4, 33].

In contrast, for strong excitation, the T_e dependence of C_e has to be taken into account, leading to a nonexponential T_e decay with a large perturbation dependent slowing down of its short time delay dynamics (Fig. 7) [4,48,49]. In this nonlinear regime, quantitative extraction of the intrinsic electron–lattice interaction parameter ($\tau^0_{\mathrm{e-ph}}$ or G) requires a precise knowledge of the injected energy and of the origin of the measured signal (i.e., if it is related to ΔT_e or Δu_e).

The electron–phonon coupling G has been determined in many bulk metals (Au, Cu, Cr, Ti, W, Nb, V, Pb, Ag, ...) using this approach [14]. The influence of the crystallinity of the metal film has also been analyzed in the case of gold, showing that the decay rate is only slightly larger for a polycrystalline than for a single-crystal film [50].

Many time-resolved optical investigations have now been performed to analyze electron–lattice coupling and its modification by the confinement in noble metal nanospheres and nanorods in different matrices

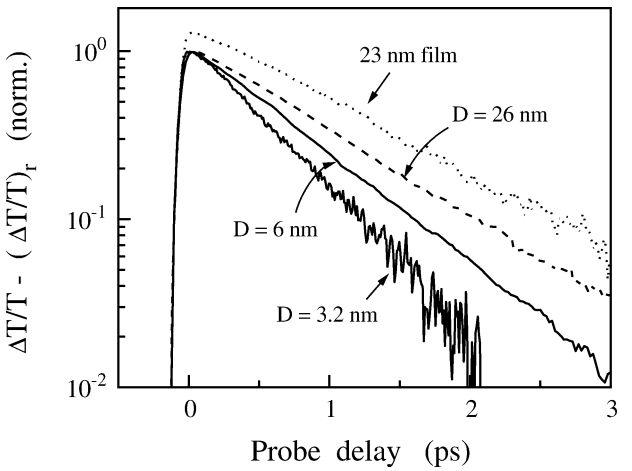

Figure 8. Time dependent transmission change measured in spherical Ag nanoparticles of diameter $D = 26$ nm and 6 nm in $BaO–P_2O_5$ and $D = 3.2$ nm in Al_2O_3, and in a 23 nm Ag film on a logarithmic scale (the latter has been up-shifted for clarity). $(\Delta T/T)_r$ is the small background long delay $\Delta T/T$. The deduced τ^0_{e-ph} are about 850, 700, 480 and 900 fs, respectively (from [56]).

or solvents, and in Ga, Sn, Pt, and Na nanoparticles [14,15]. There is, however, a large scattering of the reported decay times for the same metal [14]. As most of the experiments were performed in the strong excitation regime, these discrepancies can be partly ascribed to the perturbation dependent slowing down of the electron gas cooling, with also a possible influence of the internal electron thermalization dynamics. This is confirmed by the results of systematic pump-power dependent measurements performed in the case of gold [15,51,52], copper [16] and silver [53,54] nanoparticles that clearly show a large increase of the observed decay time τ_{e-ph} with the pump power. The intrinsic low perturbation values, τ^0_{e-ph}, of τ_{e-ph}, and thus the e–ph coupling constants $G = C_e(T_0)/\tau^0_{e-ph}$ (9), inferred by these systematic studies are consistent with those reported in films [2–4,9,55].

The intrinsic energy exchange time τ^0_{e-ph} can be directly determined in the weak perturbation regime with probing well below Ω_{ib}. In agreement with the two-temperature model (9), exponential decays of the transmission changes have then been observed for silver and gold (Fig. 8). Measurements performed for D ranging from 4.2 to 30 nm have shown that τ^0_{e-ph} is comparable to its bulk value ($\tau^0_{e-ph} \approx 0.85$ ps in Ag) for large nanoparticles ($D \geqslant 10$ nm, typically) but significantly decreases for smaller ones (with $\tau^0_{e-ph} \sim 0.6$ ps for $D = 4.2$ nm in Ag) [56]. In contrast, using extrapolation of the strong perturbation measurements, no size dependence of τ^0_{e-ph} (or G) has been estimated in the case of gold colloidal nanoparticles with sizes between 2.4 and 100 nm by Hartland et al. [52,57]. A similar conclusion was drawn by El-Sayed et al. for radii ranging from 2 to 50 nm [15]. A nonmonotonic size dependence has been observed by Zhang et al. in gold [58] with possible modification of the decay time due to strong excitation.

A decrease of the $\Delta T/T$ decay time with D has also been reported in tin [59] and gallium [19] nanoparticles for sizes ranging from 4 to 12 nm and 10 to 18 nm, respectively. The size dependence is however much larger than for silver, τ_{e-ph} being almost proportional to D over the investigated range. This variation has been interpreted in term of electron coupling with the surface acoustic modes of the particles (i.e., the quantized vibration modes replacing the bulk ones, Section 7) and quenching of the electron-bulk phonon interactions using the Belotskii and Tomchuk model [60,61]. However, this model, only applicable to small sizes, predicts a much slower electron–lattice energy transfer than in the bulk [61], in contrast to the observations in noble metals.

The origin of the different behavior observed by the different groups and the actual size dependence of the electron–lattice energy exchanges is not clear. However, the observation of a τ^0_{e-ph} size dependence in silver, similar to that of τ_{th}, suggests a confinement induced acceleration of these exchanges due to the increase of the electron–lattice mode coupling as in semiconductor nanoparticles [62]. An important point here could be the influence of the environment [13,45,63], and of the interface layer and quality (as has

been observed for the SPR width [29]). This can be particularly important for small sizes for which the particles are strongly coupled with their environment, the ratio of the surface to volume atom numbers strongly increasing as D decrease. Actually, the decay times measured in 18 nm gold particles have been shown to depend on the solvent (water or cyclohexane) [63]. Similarly, relaxation has been found to be faster in Ag particles embedded in aluminate than in silica glass [45]. Though both of these measurements were performed in the strong excitation regime, a similar matrix effect could affect the weak perturbation studies. An important effect could be local heating of the matrix around the nanoparticles with thus a strong influence of the thermal conductivity of the matrix material [13]. Additional experimental and theoretical investigations are clearly needed to understand electron–lattice coupling in confined metallic systems.

7. Acoustic vibration of clusters

The vibrational atomic motion in bulk crystals is described in terms of phonons. This approach assumes translational invariance and can be used only if the object size is much larger than the spatial extension of the phonon, i.e., its wavelength λ_{ph}. When it becomes comparable to λ_{ph} the interfaces impose new boundary conditions, i.e., new quantization conditions, on the vibrational eigenmodes. For acoustic modes, the low frequency phonons ($\omega_{\mathrm{ph}} = 2\pi v_s/\lambda_{\mathrm{ph}}$) are first altered with the appearance of discrete acoustic vibration modes, while the high frequency (i.e. small wavelength with $\lambda_{\mathrm{ph}} \ll R$) phonons are almost unaffected [64–68]. The quantized mode properties, frequency and damping, reflect the size, shape and environment of the particles. Their investigation can thus bring important information on the intrinsic elastic properties of the clusters (sound velocity, density, ...), on the composite material properties (shape of the constituting particle, interface quality, presence of adsorbed molecules...) and on particle–matrix energy transfers which is an essential parameter for the development of practical devices.

For not too small nanoobjects (typically $D \geqslant 2$ nm for a sphere) a 'macroscopic' description of the particle, neglecting its atomic structure, can be used. This is justified by the fact that the low frequency acoustical modes are associated to spatial displacements on scales much larger than the interatomic distance. They are thus described as the vibration eigenmodes of a isotropic homogeneous body in an homogeneous environment [64–68]. In time-resolved experiments, only the radial eigenmodes, that correspond to isotropic atomic displacement of a sphere, are observed [69]. For a weak coupling with the matrix, the n-th radial mode frequency is given by [69,70]:

$$\omega_n \approx 2\pi(n+1)\frac{v_L^{(s)}}{D} \tag{10}$$

where $v_L^{(s)}$ is the longitudinal sound velocity in the sphere. It is weakly sensitive to the environment and almost corresponds to the phonon mode satisfying the proper spatial condition, i.e., $\lambda_{\mathrm{ph}} = D/(n+1)$.

In contrast, the damping rate γ_n is very sensitive to the environment (type of solvent or glass). It is essentially determined by the acoustic impedance mismatch [69,70]:

$$\gamma_n \approx \frac{\rho^{(m)}}{\rho^{(s)}}\frac{v_L^{(m)}}{R} \tag{11}$$

This is a direct consequence of the intrinsic damping mechanism of the radial vibrations. The sphere movement is associated to an expanding spherical wave in the matrix reflecting energy transfer at the metal-matrix interface [67]. This makes it a sensitive local probe of the environment and interface (presence of an interface layer, solvent, type of glass, ...) and of the matrix elasto-acoustic properties.

In experiments, a large ensemble of nanoparticles dispersed in a matrix is studied. For a weak density of randomly distributed nanoparticles, their coupling can be neglected and the above single sphere model can be generalized, taking into account the size dispersion. The frequency of the vibrational modes of

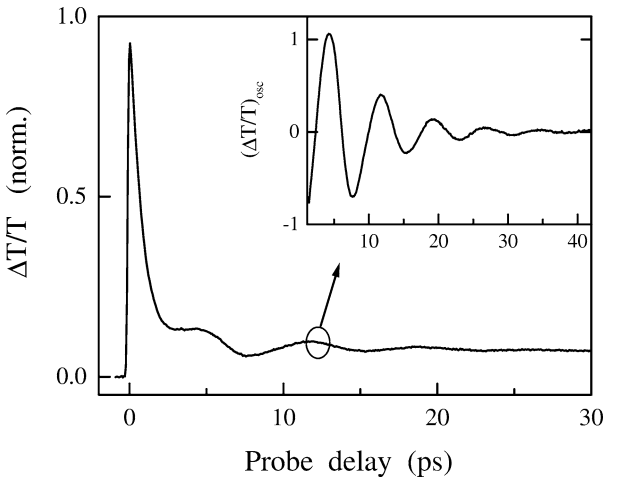

Figure 9. Transmission change $\Delta T/T$ measured in $D = 24$ nm Ag nanoparticles in glass around the surface plasmon resonance ($\hbar\omega_{\mathrm{pr}} = 2.95$ eV). The inset shows the oscillating part of the signal on an enlarged scale, with an oscillation period of 7.6 ps (from [78]).

nanoparticles has been studied using spontaneous Raman scattering [71–74] but no information has been obtained on their damping. This is difficult to address in the spectral domain, especially in the case of metallic systems, because of the low frequency and large damping of these modes. The vibrations of nanoparticles can be detected in the time domain if they are all excited and subsequently oscillating in phase. Such investigations have been recently reported in semiconductor [75,76] and metal clusters [51, 57,69,77–79], permitting to analyze not only the frequency but also the damping of the breathing modes [78,76].

In metal nanoparticles, one takes advantage of the enhancement of the nonlinear response in the vicinity of the SPR to detect their vibration. Experimentally, they show-up as a modulation of $\Delta T/T$ on a few picosecond time scale (Fig. 9). It has been shown that these essentially reflect modulation of the SPR frequency by the fundamental mode $n = 0$ that corresponds to a periodic expansion and contraction of the whole sphere (Fig. 10) [69,78,79]. In this process, the electronic properties of each nanosphere adiabatically follow the lattice sphere movement, leading to a modulation of the real part of the metal particle dielectric function, consistent with the results obtained for the expansion mode of metal films [79]. In the case of glass embedded clusters, a good agreement between the measured and calculated frequencies has been found (Fig. 10) [78], while in colloidal solutions a smaller frequency has been observed due to the accompanying movement of the stabilizing molecules bounded to the sphere surface [80].

The fact that the fundamental radial mode dominates the response has been attributed to the isotropy of the excitation process mediated by lattice expansion [69]. Excitation can be related to the fast creation of a thermal stress due to electron excitation, either directly (electron pressure) or indirectly after electron energy transfer to the lattice (lattice anharmonicity) [81]. Both effects are related to the metal dilatation and displace the equilibrium size, D_{eq}, of the spheres much faster than the breathing mode period (or equivalently the characteristic time for the sphere surface movement). Their size start increasing simultaneously and subsequently oscillate around their new equilibrium value: the breathing mode is impulsively launched with a well defined phase. The phase of the observed oscillation is a signature of the excitation process which has been shown to be dominated by the indirect mechanism [69].

A single mode dominating the time domain response, its intrinsic damping, τ_h, can be determined from the observed oscillation damping, taking into account the nanoparticle size dispersion [78]. For narrow size dispersion and a glass matrix, the intrinsic damping is sufficiently large to dominate and τ_h can thus be precisely determined [78]. The experimental values of τ_h are, however, significantly larger than the theoretical ones calculated assuming the metal–glass interface to be perfect (i.e., a perfect continuity is assumed) (Fig. 10). This discrepancy has been ascribed to metal–glass interface defects and/or the existence of an interface layer that decreases its coupling to the matrix [78]. This sensitivity of τ_h on the metal-

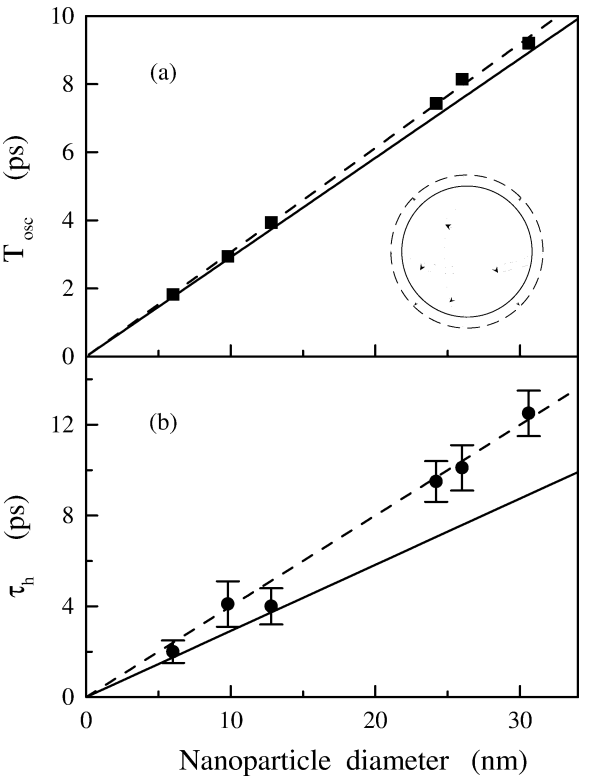

Figure 10. (a) Measured oscillation period T_{osc} as a function of the Ag nanoparticle diameter. The lines show the computed period $2\pi/\omega_0$ of the breathing mode (schematically shown at the figure bottom) for free (dashed line) and $BaO–P_2O_5$ (full line) embedded Ag nanoparticles. (b) Measured homogeneous damping time τ_h as a function of R. The dashed line is a fit and the full line the damping time $\tau_0 = 1/\gamma_0$ computed for a perfect nanoparticle–matrix contact.

matrix interface quality provides a unique way to test nanoparticle fabrication procedures and sample quality.

The situation is different for a softer environment, as in the case of colloids, where, because of the large acoustic mismatch, the intrinsic damping is much weaker. The oscillation decay is thus dominated by an inhomogeneous type of damping: the different nanoparticle having slightly different sizes, they oscillate with different frequencies and thus drift out of phase with time, their contribution eventually interfering destructively. A good correlation between the apparent damping time and the measured size distribution has then been obtained [51,57].

If it is possible to impulsively launch a vibration mode, it is also possible to control its amplitude using a multiple excitation scheme. This is also the case for the ensemble of local oscillators formed by the nanoparticles whose mechanical movement can thus be optically controlled [79]. This has been demonstrated in the simplest situation of two pump-pulses delayed by half the oscillation period $\Delta t_{\mathrm{pump}} = T_{\mathrm{osc}}/2$: expansion of the spheres is launched by the first pulse and stopped by the second one. This approach has recently been used to manipulate the mechanical movement of nanosphere, blocking the fundamental $n = 0$ mode and launching the much weaker higher order radial modes ($n \geqslant 1$).

8. Conclusions

Time resolved experiments have emerged as powerful tools for the selective investigation of electron kinetics in metals, offering the unique possibility of separating the different elementary electron interaction processes. With their recent extensions and the improvement of the femtosecond lasers, they now offer the unique possibility to directly address these problems in metal clusters. The first results, mostly obtained in noble metal clusters, are very promising and have already yielded new insights into the impact of

confinement on the electron kinetics and the first steps of its evolution form a bulk-like to a molecular type of behavior.

Results have now been obtained on electron–electron and electron–phonon scattering in noble metal particles over very large size ranges and for different type of environment. Electron–electron energy exchanges have been shown to be almost unaffected by confinement for sizes larger than 10 nm and to strongly increase for smaller sizes. Extension of these first measurements to other metals or type of confinement (1D or 2D systems) and the use of other techniques, such as time-resolved photoemission [44] would be particularly interesting here. The size dependence of electron–lattice energy exchanges is still controversial, probably because of the influence of the surrounding media and/or difficulty of comparing experiments performed in very different conditions. Further systematic investigations are clearly necessary, in particular as a function of the environment. A very interesting extension of these type of measurements would be the time-resolved investigation of spin dynamics in clusters, similarly to what has been done in bulk metals [82–84]. On the theoretical side, the electron dynamics modeling is based on a small solid approach, i.e., modifications are introduced to the bulk material response. This is justified for not too small clusters, formed by more than few hundred atoms, for which quantum mechanical confinement only introduces corrections to their properties, but only constitutes a first approximation. Improved modeling of the electron scattering based on a quantum mechanical approach is necessary for understanding electron interactions in a confined system.

Time-resolved techniques also offer new possibilities for the investigation and control of the coherent acoustic vibration of metal nanoparticles. This approach turn-out to be fully complementary with the Raman scattering technique, since, when directly following cluster vibration in the time domain, both the frequency an damping of their fundamental breathing mode can be determined. Their environment directly reflects in the measured damping, which is very sensitive to the nature of the surrounding media and interface quality, making clusters a local probe of their environment. This is related to the general problem of energy at a heterogeneous interface, whose understanding is essential for the engineering and application of these systems. Optical coherent control of the electronic excitation and relaxation in metal is also certainly at its first steps, and opens-up a new field of ultrafast studies in metals.

Up to now all the experimental studies were performed on an ensemble of nanoparticles (a few tens of thousand to one million, typically) embedded in a matrix or deposited on a substrate. The responses are thus averaged over their size distribution and environment fluctuation. This is imposed by experimental constraints: the limited spatial resolution and measurement sensitivity. Improvement of the experimental techniques should permit us to address nanoparticle dynamics in different conditions, such as those of free clusters or of an individual cluster. In particular, using near field optical microscopy, linear spectroscopy of individual metal nanoparticles has been recently reported [85]. Extension of these technique to the time domain, as was done in the case of semiconductor wires is very interesting [86,87]. This should permit a closer comparison of the experimental and theoretical results, bringing new insight into the understanding of the physics of these systems.

On the other hand, most of the measurements were performed in relatively dilute material for which cluster coupling can be neglected. High density and, in particular, 2D and 3D self-organized nanoparticle systems can now be grown and are known to exhibit collective properties [88–92]. Study of the impact of this coupling on their dynamics, energy and charge exchange processes, and optical nonlinearities is a very promising new area.

Acknowledgements. We wish to thank C. Voisin, D. Christofilos and C. Flytzanis for their important contributions to these studies and for very helpful discussions. We are also indebted to A. Nakamura, Y. Hamanaka, S. Omi for helpful discussions and for providing some of the silver nanoparticle samples. We also thank B. Prével, M. Gaudry, E. Cottancin, J. Lermé, M. Pellarin, M. Broyer, M. Maillard and M. P. Pileni for their help in the theoretical and experimental parts of this work and for providing us with very good quality samples. We also acknowledge financial support by the Conseil Régional d'Aquitaine.

To cite this article: N. Del Fatti, F. Vallée, C. R. Physique 3 (2002) 365–380

References

[1] F. Vallée, C. R. Acad. Sci. 2 (2001) 1469.
[2] C.K. Sun, F. Vallée, L.H. Acioli, E.P. Ippen, J.G. Fujimoto, Phys. Rev. B 50 (1994) 15337.
[3] R. Groeneveld, R. Sprik, A. Lagendijk, Phys. Rev. B 51 (1995) 11433.
[4] N. Del Fatti, C. Voisin, M. Achermann, S. Tzortzakis, D. Christofilos, F. Vallée, Phys. Rev. B 61 (2000) 16956.
[5] W.S. Fann, R. Storz, H.W.K. Tom, J. Bokor, Phys. Rev. Lett. 68 (1992) 2834; Phys. Rev. B 46 (1992) 13592.
[6] A. Knoesel, A. Hotzel, M. Wolf, Phys. Rev. B 57 (1998) 12812.
[7] M. Aeschlimann, M. Bauer, S. Pawlik, W. Weber, R. Burgermeister, D. Oberli, H.C. Siegmann, Phys. Rev. Lett. 79 (1997) 5158.
[8] S. Ogawa, H. Nagano, H. Petek, Phys. Rev. B 55 (1997) 10869.
[9] S.D. Brorson, A. Kazeroonian, J.S. Modera, D.W. Face, T.K. Cheng, E.P. Ippen, M.S. Dresselhaus, G. Dresselhaus, Phys. Rev. Lett. 64 (1990) 2172.
[10] N. Del Fatti, R. Bouffanais, F. Vallée, C. Flytzanis, Phys. Rev. Lett. 81 (1998) 922.
[11] C. Flytzanis, F. Hache, M.C. Klein, D. Ricard, P. Roussignol, in: E. Wold (Ed.), Progress in Optics, Vol. XXIX, North-Holland, Amsterdam, 1991, p. 321.
[12] M.J. Bloemer, J.W. Haus, P.R. Ashley, J. Opt. Soc. Am. B 7 (1990) 790.
[13] R.F. Haglund, G. Lupke, D.H. Osborne, H. Chen, R.H. Magruder, R.A. Zuhr, in: T. Elsaesser, J.G. Fujimoto, D.A. Wiersma, W. Zinth (Eds.), Ultrafast Phenomena XI, Springer-Verlag, Berlin, 1998, p. 356.
[14] For a review see, C. Voisin, N. Del Fatti, D. Christofilos, F. Vallée, J. Phys. Chem. B 105 (2001) 2264.
[15] S. Link, M.A. El-Sayed, J. Phys. Chem. B 103 (1999) 8410.
[16] T. Tokizaki, A. Nakamura, S. Kavelo, K. Uchida, S. Omi, H. Tanji, Y. Asahara, Appl. Phys. Lett. 65 (1994) 941.
[17] J.Y. Bigot, J.C. Merle, O. Cregut, A. Daunois, Phys. Rev. Lett. 75 (1995) 4702.
[18] M. Perner, P. Bost, U. Lemmer, G. von Plessen, J. Feldmann, U. Becker, M. Mennig, M. Schmitt, H. Schmidt, Phys. Rev. Lett. 78 (1997) 2192.
[19] M. Nisoli, S. Stagira, S. De Silvestri, A. Stella, P. Tognini, P. Cheyssac, R. Kofman, Phys. Rev. Lett. 78 (1997) 3575.
[20] N. Del Fatti, F. Vallée, F.C. Flytzanis, Y. Hamanaka, A. Nakamura, Chem. Phys. 251 (2000) 215.
[21] N. Del Fatti, F. Vallée, Appl. Phys. B 73 (2001) 283.
[22] A. Kawabata, R. Kubo, J. Phys. Soc. Jap. 21 (1966) 1765.
[23] L. Genzel, T.P. Martin, U. Kreibig, Z. Phys. B 21 (1975) 339.
[24] U. Kreibig, M. Vollmer, Optical Properties of Metal Clusters, Springer, Berlin, 1995.
[25] F. Vallée, N. Del Fatti, C. Flytzanis, in: V.M. Shalaev, M. Moskovits (Eds.), Nanostructured Materials, American Chemical Society, Washington, 1997, p. 70.
[26] P.B. Johnson, R.W. Christy, Phys. Rev. B 6 (1972) 4370.
[27] N.W. Ashcroft, N.D. Mermin, Solid State Physics, Holt–Saunders, Tokyo, 1981.
[28] F. Hache, D. Ricard, C. Flytzanis, C. J. Opt. Soc. Am. B 3 (1986) 1647.
[29] H. Hovel, S. Fritz, A. Hilger, U. Kreibig, M. Vollmer, Phys. Rev. B 48 (1993) 18178.
[30] B. Lamprecht, A. Leitner, F.R. Aussenegg, Appl. Phys. B 68 (1999) 419.
[31] B. Lamprecht, J.R. Krenn, A. Leitner, F.R. Aussenegg, Phys. Rev. Lett. 83 (1999) 4421.
[32] T. Vartanyan, M. Simon, F. Träger, Appl. Phys. B 68 (1999) 425.
[33] C. Voisin, D. Christofilos, N. Del Fatti, F. Vallée, Eur. Phys. J. D 16 (2001) 139.
[34] R. Matzdorf, A. Gerlach, F. Theilmann, G. Meister, A. Goldmann, Appl. Phys. B 68 (1999) 393.
[35] J.M. Ziman, Principles of the Theory of Solids, Cambridge University Press, Cambridge, 1969.
[36] R. Knorren, K.H. Bennemann, R. Burgermeister, M. Aeschlimann, Phys. Rev. B 61 (2000) 9427.
[37] R. Rosei, C.H. Culp, J.H. Weaver, Phys. Rev. B 10 (1974) 484.
[38] C. Voisin, D. Christofilos, N. Del Fatti, F. Vallée, B. Prével, E. Cottancin, J. Lermé, M. Pellarin, M. Broyer, Phys. Rev. Lett. 85 (2000) 2200.
[39] D. Pines, P. Nozières, The Theory of Quantum Liquids, Benjamin, New York, 1966.
[40] W. Ekardt, Phys. Rev. B 29 (1984) 1558.
[41] C. Bréchignac, P. Cahuzac, J. Leygnier, A. Sarfati, Phys. Rev. Lett. 70 (1993) 2036.
[42] A. Liebsch, Phys. Rev. B 48 (1993) 11317.
[43] J. Lermé, B. Palpant, B. Prével, M. Pellarin, M. Treilleux, J.L. Vialle, A. Perez, M. Broyer, Phys. Rev. Lett. 80 (1998) 5105.
[44] M. Fierz, K. Siegmann, M. Scharte, M. Aeschlimann, Appl. Phys. B 68 (1999) 415.
[45] V. Halté, J.Y. Bigot, B. Palpant, M. Broyer, B. Prével, A. Pérez, Appl. Phys. Lett. 75 (1999) 3799.
[46] Y. Hamanaka, J. Kuwabata, I. Tanahashi, S. Omi, A. Nakamura, Phys. Rev. B 63 (2001) 104 302.

[47] M.I. Kaganov, I.M. Lifshitz, L.V. Tanatarov, Zh. Eksp. Teor. Fiz. 31 (1957) 232 [Sov. Phys. JETP 4 (1957) 173].
[48] R.W. Schoenlein, W.Z. Lin, J.G. Fujimoto, G.L. Eesley, Phys. Rev. Lett. 58 (1987) 1680.
[49] C.K. Sun, F. Vallée, L.H. Acioli, E.P. Ippen, J.G. Fujimoto, Phys. Rev. B 48 (1993) 12365.
[50] H.E. Elsayed-Ali, T. Juhasz, G.O. Smith, W.E. Bron, Phys. Rev. B 43 (1991) 4488.
[51] J.H. Hodak, I. Martini, G.V. Hartland, J. Phys. Chem. B 102 (1998) 6958.
[52] J.H. Hodak, A. Henglein, G.V. Hartland, J. Chem. Phys. 112 (2000) 5942.
[53] V. Halte, J. Guille, J.-C. Merle, I. Perakis, J.-Y. Bigot, Phys. Rev. B 60 (1999) 11738.
[54] Y. Hamanaka, A. Nakamura, S. Omi, N. Del Fatti, F. Vallée, C. Flytzanis, Appl. Phys. Lett. 75 (1999) 1712.
[55] D. Liu, P. He, D.R. Alexander, Appl. Phys. Lett. 62 (1993) 249.
[56] N. Del Fatti, C. Flytzanis, F. Vallée, Appl. Phys. B 68 (1999) 433.
[57] J.H. Hodak, A. Henglein, G.V. Hartland, J. Chem. Phys. 111 (1999) 8613.
[58] B.A. Smith, J.Z. Zhang, U. Giebel, G. Schmid, Chem. Phys. Lett. 270 (1997) 139.
[59] A. Stella, M. Nisoli, S. De Silvestri, O. Svelto, G. Lanzani, P. Cheyssac, R. Kofman, Phys. Rev. B 53 (1996) 15497.
[60] E.D. Belotskii, P.M. Tomchuk, Surf. Science 239 (1990) 143.
[61] E.D. Belotskii, P.M. Tomchuk, Int. J. Electr. 73 (1992) 955.
[62] T. Takagahara, J. Lum. 70 (1996) 129.
[63] J.Z. Zhang, Acc. Chem. Res. 30 (1997) 423.
[64] H. Lamb, Proc. London Math. Soc. 13 (1882) 189.
[65] A. Tamura, T. Ichinokawa, J. Phys. C 16 (1983) 4779.
[66] N. Nishiguchi, T. Sakuma, Sol. State Comm. 38 (1981) 1073.
[67] V.A. Dubrovskiy, V.S. Morochnik, Earth Phys. 17 (1981) 494.
[68] Y. Satô, T. Usami, Geophys. Mag. 31 (1962) 15.
[69] C. Voisin, N. Del Fatti, D. Christofilos, F. Vallée, Appl. Surf. Science 164 (2000) 131.
[70] C. Voisin, D. Christofilos, N. Del Fatti, F. Vallée, Physica B (to be published).
[71] L. Saviot, B. Champagnon, E. Duval, A.I. Ekimov, Phys. Rev. B 57 (1998) 341, and references therein.
[72] M. Fujii, T. Nagareda, S. Hayashi, K. Yamamoto, Phys. Rev. B 44 (1991) 6243.
[73] N. Felidj, J. Aubard, G. Lévi, J. Chem. Phys. 104 (1996) 9735.
[74] H. Portales, L. Saviot, E. Duval, M. Fujii, N. Del Fatti, F. Vallée, J. Chem. Phys. 115 (2001) 3444.
[75] T.D. Krauss, F.W. Wise, Phys. Rev. Lett. 79 (1997) 5102.
[76] E.R. Thoen, G. Steinmeyer, P. Langlois, E.P. Ippen, G.E. Tudury, C.H. Brito Cruz, L.C. Barbosa, C.L. Cesar, Appl. Phys. Lett. 73 (1998) 2149.
[77] M. Nisoli, S. De Silvestri, A. Cavalleri, A.M. Malvezzi, A. Stella, G. Lanzani, P. Cheyssac, R. Kofman, Phys. Rev. B 55 (1997) R13424.
[78] N. Del Fatti, C. Voisin, F. Chevy, F. Vallée, C. Flytzanis, J. Chem. Phys. 110 (1999) 11484.
[79] N. Del Fatti, C. Voisin, D. Christofilos, F. Vallée, C. Flytzanis, J. Phys. Chem. A 104 (2000) 4321.
[80] C. Voisin, Ph.D. Thesis, Orsay University, 2001.
[81] T.H.K. Barron, J.G. Collins, G.K. White, Adv. Phys. 29 (1980) 609.
[82] E. Beaurepaire, J.C. Merle, A. Daunois, J.Y. Bigot, Phys. Rev. Lett. 76 (1996) 4250.
[83] J. Hohlfeld, E. Matthias, R. Knorren, K.H. Bennemann, Phys. Rev. Lett. 78 (1997) 4861.
[84] G. Ju, A. Vertikov, A.V. Nurmikko, C. Canady, G. Xiao, R.F.C. Farrow, A. Cebollada, Phys. Rev. B 57 (1998) R700.
[85] T. Klar, M. Perner, S. Grosse, G. Von Plessen, W. Spirkl, J. Feldmann, Phys. Rev. Lett. 80 (1998) 4249.
[86] B.A. Nechay, U. Siegner, F. Morier-Genoud, A. Schertel, U. Keller, Appl. Phys. Lett. 74 (1999) 61.
[87] T. Guenther, V. Emiliani, F. Intonti, C. Lienau, T. Elsaesser, R. Nötzel, K.H. Ploog, Appl. Phys. Lett. 75 (1999) 3500.
[88] V.M. Shalaev, Phys. Rep. 272 (1996) 61.
[89] A. Taleb, C. Petit, M.P. Pileni, Chem. Mater. 9 (1997) 950.
[90] J.R. Krenn, A. Dereux, J.C. Weeber, E. Bourillot, Y. Lacroute, J.P. Goudonnet, G. Schider, W. Gotschy, A. Leitner, F.R. Aussenegg, C. Girard, Phys. Rev. Lett. 82 (1999) 2590.
[91] B. Lamprecht, G. Schider, R.T. Lechner, H. Ditlbacher, J.R. Krenn, A. Leitner, F.R. Aussenegg, Phys. Rev. Lett. 84 (2000) 4721.
[92] F. Silly, A.O. Gusev, A. Taleb, F. Charra, M.P. Pileni, Phys. Rev. Lett. 84 (2000) 5840.